Adaptive radar approaches for Doppler moments estimation

Pappas, Apostolos; Dash, Tworit; Yarovoy, Alexander; Fioranelli, Francesco; Sardar, Shafi; Schleiss, Marc

DOI
10.1109/LGRS.2025.3646459

Publication date
2026

Document Version
Final published version

Published in
IEEE Geoscience and Remote Sensing Letters

Adaptive Radar Approaches for Doppler Moment Estimation

Apostolos Pappas, *Graduate Student Member, IEEE*, Tworit Dash, *Member, IEEE*, Alexander Yarovoy, *Fellow, IEEE*, Francesco Fioranelli, *Senior Member, IEEE*, Shafi Sardar, and Marc Schleiss

***Abstract*—To characterize atmospheric turbulence, the Doppler moments are estimated by weather radars. However, moment accuracy is highly sensitive to radar transmission parameters such as the pulse repetition time (T_s) and the number of pulses (N_p), which affects Doppler ambiguity and estimation variance. Traditional fixed-parameter radars face tradeoffs between aliasing and measurement precision. This letter proposes an adaptive radar framework that dynamically adjusts T_s and N_p on a per-scan basis to improve Doppler moment estimation at a single resolution cell level. Inspired by the fully adaptive radar (FAR) concept, the method also includes a novel multilag Doppler width estimation scheme. Results demonstrate enhanced estimation accuracy, enabling better responsiveness to localized and nonstationary weather conditions.**

***Index Terms*—Adaptive radar, Doppler moment estimation, weather radar.**

I. Introduction

WEATHER radar systems are essential for monitoring atmospheric phenomena, enabling accurate detection and characterization of precipitation, storms, and other meteorological events [1], [2]. A fundamental capability of weather radars is the estimation of Doppler moments, i.e., reflectivity, mean radial velocity, and spectral width within each resolution volume defined by azimuth, range, and elevation. These moments offer key insights into the intensity, motion, and turbulence of hydrometeors, enhancing weather forecasting.

The first Doppler moment, radial velocity, represents the mean hydrometeor motion along the radar beam, while the square root of the second central moment, spectral width, reflects the velocity dispersion due to turbulence and other microphysical processes. These estimates are often challenged by velocity ambiguities, especially in nonstationary and spatially heterogeneous weather conditions. A key limitation of traditional radars is the use of fixed T_s and N_p settings. Although such configurations may work under stationary or quasi-stationary conditions, they are suboptimal in rapidly changing environments. For example, in the vicinity of airports, rapidly evolving phenomena, such as wind shear, microbursts, and gust fronts, can develop within a few tens of seconds and pose serious hazards to aircraft while taking off and landing. Therefore, an adaptive strategy aiming to update the parameters T_s and N_p from scan to scan is essential to capture rapid changes while maintaining situational awareness.

The accuracy of Doppler moment estimation depends heavily on both the quality of the received signal and the radar transmission parameters. Key factors include the signal-to-noise ratio (SNR), the *pulse repetition time* (T_s), the *number of integrated pulses* (N_p), and the statistical properties of the returned echoes. High SNR is essential, particularly for reliable spectral width estimates, while the choice of T_s directly affects the maximum unambiguous velocity and the risk of Doppler velocity aliasing. The parameter N_p controls the coherent processing interval (CPI; i.e., $N_p \times T_s$ per range-resolution volume) and by extension, the Doppler resolution. A poor choice of N_p can significantly bias the Doppler moments. Optimal moment estimation, thus, requires careful tuning of these radar parameters to match the precipitation dynamics within each resolution cell.

According to the theory, a shorter T_s improves maximum unambiguous velocity but increases the estimation variance of the moments [3], while a longer T_s reduces variance but increases aliasing risk. Similar tradeoffs apply to the number of integrated pulses. To overcome these limitations, adaptive radar systems dynamically adjust parameters such as T_s and N_p in response to real-time measurements. This adaptive capability can be beneficial when estimating moments within a single resolution cell, where local weather conditions may deviate significantly from broader trends. Here, we propose an adaptive radar framework that modifies T_s and N_p scan-by-scan to balance the tradeoffs between aliasing and estimation variance. We focus on a single azimuth–range–elevation cell, providing a foundation for future large-scale extensions to include the whole field of view. The key contributions are given as follows.

1) We define a novel adaptation scheme for a single resolution cell inspired by the adaptation pipeline of the fully adaptive radar (FAR) framework [4].
2) We employ the adaptation of multilag estimation of Doppler width for improved estimation performance of the moments.

The rest of this letter is structured as follows. Section II introduces the signal model, and Section III introduces the

Received 4 September 2025; revised 3 December 2025; accepted 13 December 2025. Date of publication 19 December 2025; date of current version 31 December 2025. This work was supported by the Dutch Research Council NWO under the Open Technology Program, Project Strategic Monitoring of Atmospheric Threats using Enhanced Radar (SMARTER). *(Corresponding author: Apostolos Pappas.)*

Apostolos Pappas, Tworit Dash, Alexander Yarovoy, and Francesco Fioranelli are with the Microwave Sensing, Signals and Systems (MS3) Group, Microelectronics Department, TU Delft, 2628CD Delft, The Netherlands (e-mail: a.pappas-2@tudelft.nl; t.k.dash@tudelft.nl; a.yarovoy@tudelft.nl; f.fioranelli@tudelft.nl).

Shafi Sardar and Marc Schleiss are with the Department of Geoscience and Remote Sensing, TU Delft, 2628CN Delft, The Netherlands (e-mail: s.s.a.sardar@tudelft.nl; m.a.schleiss@tudelft.nl).

Digital Object Identifier 10.1109/LGRS.2025.3646459

estimation of Doppler moments using the pulse-pair (PP) method. Section IV presents the proposed adaptation scheme with results given in Section V, and conclusions are drawn in Section VI.

II. Signal Model

Consider a radar resolution volume containing M raindrops during a rain event. At any given time step t_n, the radar echo received is the result of the coherent superposition of the individual echoes scattered by each of these raindrops [5]

$$s(t_n) = \sum_{m=1}^{M} A_m \exp(j\beta_m) \exp\left(j\frac{4\pi}{\lambda} v_{m,r} t_n\right) \tag{1}$$

where A_m is the amplitude related to the mth scatterer, j is the imaginary unit, i.e., $(-1)^{1/2}$, and λ is the central wavelength calculated as c/f_c with f_c being the radar center frequency and c being the speed of electromagnetic (EM) waves. Finally, $v_{m,r}$ is the radial velocity of the mth scatterer at time t_n. The factor $\exp(j\beta_m)$ represents the initial phase shift introduced by the incoming EM wave, which is a function of the initial position of the scatterer. Scatterers are assumed to have equal size, i.e., $A_m = A$, independent and identically distributed (i.i.d.) initial phases with a uniform distribution ($\beta_m \overset{\text{i.i.d.}}{\sim} \mathcal{U}[-\pi, +\pi]$) and i.i.d. Gaussian-distributed velocities ($v_{m,r} \overset{\text{i.i.d.}}{\sim} \mathcal{N}(\mu_v, \sigma_v^2)$). The parameters μ_v and σ_v are the mean radial velocity and the radial velocity dispersion (the parameters of interest). The equality of all scatterers' amplitudes is such that it does not interfere with the assumptions on the Gaussian nature of the power spectrum for sufficiently large M.

Finally, zero-mean complex white Gaussian noise $\boldsymbol{\eta}$ is added to the measured signal $\mathbf{s}$. Let $\mathbf{y}, \mathbf{s}, \boldsymbol{\eta} \in \mathbb{C}^{N_p}$ denote vectors, with $\mathbf{y}$ being the total measured signal with noise

$$\mathbf{y} = \mathbf{s} + \boldsymbol{\eta}, \quad \boldsymbol{\eta} \sim \mathcal{CN}(\mathbf{0}, \sigma_\eta^2 \mathbf{I}_{N_p}). \tag{2}$$

This is the measured signal to be used for all estimation, tracking, and adaptation tasks described in this work.

III. Estimation of Doppler Moments

To estimate the Doppler moments, we make use of the nonparametric and computationally efficient PP, or autocovariance [2], [3], method, a well-known and used time-domain technique to estimate the Doppler moments. Moreover, the PP method for the spectral width is aliasing invariant.

Let $y[n]$ (for compact notation, we use n instead of t_n from now on) denote the complex radar return at pulse index n, for $n = 0, 1, \ldots, N_p - 1$. The signal is assumed to be a wide-sense stationary proper Gaussian process with a Doppler spectrum centered at a mean frequency $f_D = 2\mu_v/(\lambda)$ and spectral width $w_D = 2\sigma_v/(\lambda)$ (both in Hz), related to the velocity parameters μ_v and σ_v. The PP method exploits the phase and magnitude of lagged autocorrelation estimates to retrieve Doppler moments. Firstly, we define the autocorrelation estimate at lag ℓ as

$$R_\ell = \frac{1}{N_p} \sum_{n=0}^{N_p-\ell-1} y^*[n] \cdot y[n+\ell] \tag{3}$$

where $y^*[n]$ denotes the complex conjugate of $y[n]$. Lag-1, lag-2, and lag-3 autocorrelations can then be computed using the appropriate ℓ value in (3). f_D is computed using the phase of the lag-1 autocorrelation

$$f_D = \frac{T_s^{-1}}{2\pi} \arg(R_1). \tag{4}$$

The spectral width can be estimated using different lag relationships, assuming knowledge of the noise variance. First, we define the total signal power, corrected for σ_η^2

$$\hat{S} = \begin{cases} \frac{1}{N_p} \sum_{n=0}^{N_p-1} |y[n]|^2 - \sigma_\eta^2, & \text{if } \frac{1}{N_p} \sum |y[n]|^2 > \sigma_\eta^2 \\ \sum_{n=0}^{N_p-1} |y[n]|^2, & \text{otherwise.} \end{cases} \tag{5}$$

Then, the Doppler spectral width estimates for different lags can be computed as follows. Note that, for instance, w_{D1} corresponds to the width estimation using $\ell = 1$

$$w_{D1} = \frac{T_s^{-1}}{\sqrt{2}\pi} \sqrt{\left|\ln\left(\frac{\hat{S}}{|R_1|}\right)\right|}, \; w_{D2} = \frac{T_s^{-1}}{\sqrt{6}\pi} \sqrt{\left|\ln\left(\frac{|R_1|}{|R_2|}\right)\right|},$$
$$w_{D3} = \frac{T_s^{-1}}{4\pi} \sqrt{\left|\ln\left(\frac{|R_1|}{|R_3|}\right)\right|}. \tag{6}$$

Each of these expressions assumes a Gaussian-shaped Doppler spectrum and relies on the exponential decay of the autocorrelation magnitude over the lags. It can be observed that $\ell = 1$ is the most robust, mainly for cases with lower mean Doppler values, while higher lag estimates provide additional resolution but are more sensitive to noise and decorrelation.

As shown later in Section IV, it is of utmost importance to employ the theoretical variance of the estimation of both the mean Doppler and its width. The variance bounds for both variables of interest are derived in [3] by use of the Fisher Information Matrix. Hence, for large SNR, narrow spectrum widths (e.g., width $wT_s \approx 0.1$) and for contiguous pairs, the theoretical variance for $\hat{f}_D$ becomes [3, Eq. (4.15)]

$$\mathbb{V}_{T_s,N_p}[\hat{f}_D] = \frac{w_D}{4\sqrt{\pi} N_p T_s}. \tag{7}$$

For Doppler width estimation at relatively high SNR, the theoretical variance is given by [3, Eq. (5.5)]

$$\mathbb{V}_{T_s,N_p}[\hat{w}_D] = \frac{3 w_D}{32\sqrt{\pi} N_p T_s} \tag{8}$$

making both variances functions of the N_p and T_s. Note that both (7) and (8) use the true Doppler width value, something that is not known a priori in reality. Thus, an approach that aims to minimize the uncertainty in the estimates should use the version of (7) and (8) where w_D is replaced with its approximated estimated/predicted counterpart, i.e., $\hat{w}_D$.

IV. CPI Adaptation Scheme

In this work, we assume the existence of an adaptive radar, able to adapt its transmission parameters as done in the FAR framework introduced in [4] and extended to accommodate different optimization schemes in [6], [7], and [8]. FAR was additionally applied to weather radar in the context of cloud profiling [9]. Based on this framework, a design of an adaptive radar is depicted in Fig. 1, comprising the usual radar hardware, a processor (including the estimator of Doppler moments and their tracking), and an optimizer module.

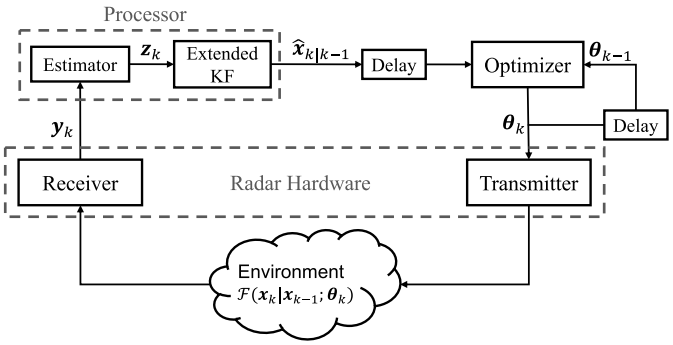

Fig. 1. Schematic representation of the proposed adaptive radar for robust estimation of Doppler moments: $\mathbf{z}_k$ represents the derived quantities after PP processing, $\mathbf{x}_k$ the state vector, and $\boldsymbol{\theta}_k$ the CPI related parameters, T_s and N_p at timestep k. The delay module tracks the temporal evolution of the system.

In our simulations, the radar performs a measurement of the target via the signal model of Section II by using certain transmit parameters $\boldsymbol{\theta} = [N_p \quad T_s]^T$. Then, the measurements are processed in the processor part of the system, where, initially, the PP method is applied, as presented in Section III, in order to estimate the Doppler moments. It is noteworthy that in this letter, measurements discussed from now on refer to the derived quantities after the PP processing, i.e., $\mathbf{z}_k = [\hat{f}_{D,k} \quad \hat{w}_{D,k}]^T$ and not the slow time raw radar echoes $y[n]$. The index (or timestep) k here refers to the scan index, each scan comprising several coherent slow time samples for Doppler processing $n = 0 \rightarrow N_p - 1$. The extended Kalman filter (EKF) also included in the processor is responsible for tracking both moments and generating predictions of the state represented as a vector, $\hat{\mathbf{x}}_{\mathbf{k|k-1}}$.

To adaptively select $\boldsymbol{\theta}$, we define the optimizer module of this adaptive radar scheme. The latter receives as input the estimation of the Doppler moments for the next timestep $k+1$ (which, by the time of transmission, are considered as a first estimation of the unknown ground truth), the measurement covariance matrix as used in the EKF module, and the currently used values of the parameters we wish to optimize. The parameter values that are derived from the optimization procedure, $\boldsymbol{\theta}_k$, are then used in the next scan. In this way, the adaptive radar system dynamically adjusts its parameters $\boldsymbol{\theta}$ to enhance the accuracy of estimating the mean Doppler velocity and Doppler spectral width while avoiding ambiguities.

In the rest of this section, we first introduce the EKF used for tracking the Doppler moments in Section IV-A. Then, in Section IV-B, we present the optimization scheme of this adaptive radar, which dictates the selection of the CPI-related radar parameters, as well as the value of the lag ℓ.

A. Tracking of Doppler Moments

In this work, we focus on adapting to a single resolution cell, i.e., a certain cell in range, azimuth, and elevation, without considering specific values of these variables. The parameters $f_{D,k}$ and $w_{D,k}$ are assumed to evolve over time through a combination of slow deterministic drift and stochastic fluctuations (modeled by the process noise of the system), reflecting the natural variability in hydrometeor motion and radar backscatter. The mean Doppler shift f_D and Doppler width w_D at timestep k are updated as follows:

$$\begin{aligned} f_D[k] &= f_D[k-1] + \alpha_f \Delta t + n_f,\ n_f \overset{\text{i.i.d.}}{\sim} \mathcal{N}(0, \sigma_f^2) \\ w_D[k] &= w_D[k-1] + \alpha_w \Delta t + n_w,\ n_w \overset{\text{i.i.d.}}{\sim} \mathcal{N}(0, \sigma_w^2) \end{aligned} \tag{9}$$

where Δt is the scan interval, α_f and α_w are drift coefficients (Hz/s), and σ_f and σ_w denote process noise standard deviations.

We consider an EKF framework for tracking f_D and w_D of a radar resolution cell. The state vector is defined as $\mathbf{x}_k = \left[f_{D,k} \ w_{D,k}\right]^\top$, with initial estimate $\mathbf{x}_0 = \left[0 \ 0\right]^\top$ and initial error covariance $\mathbf{P}$ empirically defined. The process noise covariance matrix is defined as $\mathbf{Q} = \text{diag}(\sigma_{q_f}^2 \cdot \Delta t^2,\ \sigma_{q_w}^2 \cdot \Delta t^2)$, where σ_{q_f} and σ_{q_w} are the process noise standard deviations for f_D and w_D, respectively.

Assuming a stationary process model in the EKF with state transition matrix $\mathbf{F} = \mathbf{I}_{2\times 2}$, the prediction step at each time step is

$$\hat{\mathbf{x}}_{k|k-1} = \mathbf{F}\hat{\mathbf{x}}_{k-1|k-1} \tag{10}$$

$$\mathbf{P}_{k|k-1} = \mathbf{F}\mathbf{P}_{k-1|k-1}\mathbf{F}^\top + \mathbf{Q}. \tag{11}$$

After the radar performs an observation, the estimates are given as $\mathbf{z}_k = \left[\hat{f}_{D,k} \ \hat{w}_{D,k}\right]^\top$. As described in Section III, the measurement noise covariance matrix is computed adaptively using information theoretic variance derived using the PP estimator (note the small change of notation here, with $\boldsymbol{\theta}_k = [T_{s,k}, N_{p,k}]$ for simplicity)

$$\mathbf{R}_{\boldsymbol{\theta}_k}[k] = \begin{bmatrix} \mathbb{V}_{\theta_k}(\hat{f}_D[k]) & 0 \\ 0 & \mathbb{V}_{\theta_k}(\hat{w}_D[k]) \end{bmatrix}. \tag{12}$$

With the observation matrix $\mathbf{H} = \mathbf{I}_{2\times 2}$, the EKF update step follows standard equations

$$\begin{aligned} \boldsymbol{\nu}_k &= \mathbf{z}_k - \mathbf{H}\hat{\mathbf{x}}_{k|k-1} \\ \mathbf{S}_k &= \mathbf{H}\mathbf{P}_{k|k-1}\mathbf{H}^\top + \mathbf{R} \\ \mathbf{K}_k &= \mathbf{P}_{k|k-1}\mathbf{H}^\top\mathbf{S}_k^{-1} \\ \hat{\mathbf{x}}_{k|k} &= \hat{\mathbf{x}}_{k|k-1} + \mathbf{K}_k\boldsymbol{\nu}_k \\ \mathbf{P}_{k|k} &= (\mathbf{I} - \mathbf{K}_k\mathbf{H})\mathbf{P}_{k|k-1}. \end{aligned} \tag{13}$$

This formulation enables adaptive tuning of the EKF measurement uncertainty (via the measurement noise covariance matrix) at each time step k, accounting for the evolving nature of the Doppler spectrum [10].

B. Parameter Optimization: Two Cases

This work considers two cases of adaptation. One adapts only the CPI-related parameters, while the second also selects an appropriate lag ℓ value for the calculation of the Doppler width, as discussed in Section III. Since the theoretical variances of both Doppler moment estimations heavily depend on T_s and N_p, tracking and predicting these two moments can be leveraged to optimize the aforementioned parameters for the next scan. As noted above, the goal of the adaptation and optimization procedure is twofold: 1) to select CPI parameters $\boldsymbol{\theta}$ such that the mean Doppler is measured unambiguously and 2) to improve or preserve the accuracy of moment estimation. This leads to a constrained optimization problem over T_s and N_p that balance estimation accuracy with the need to

maintain an unambiguous Doppler range sufficient to estimate f_D without aliasing.

To proceed with the optimization, we define a cost function to be minimized. As seen from (12), the trace of the measurement noise covariance matrix can serve as an appropriate objective for CPI adaptation. This choice captures both parameters of interest, and minimizing the approximate theoretical variances of the Doppler moments improves estimation quality. The approximate theoretical variances in (7) and (8) involve the EKF prediction $\hat{w}_{D,k|k-1}$ from $\hat{\mathbf{x}}_{k|k-1}$ instead of the unknown ground truth.

Similarly, the constraint imposed by aliasing avoidance is based on the predicted mean Doppler $\hat{f}_{D,k|k-1}$, requiring that $T_s \leq 1/(2|\hat{f}_{D,k|k-1}|)$. However, due to prediction uncertainty, this could lead to aliasing and degraded estimation. To mitigate this, a guard factor $\gamma \geq 1$ is introduced to tolerate prediction errors. The constant nature of γ provides a conservative guard when EKF uncertainty is unreliable (e.g., during initialization or transient regimes) [11]. While integrating EKF prediction errors into γ could tighten constraints, fixing γ is an intentional simplification chosen to preserve robustness. This gives

$$T_s \leq \frac{1}{2\gamma \cdot |\hat{f}_{D,k|k-1}|}. \tag{14}$$

Letting $\mathcal{G}(T_s, N_p, \hat{w}_{D,k|k-1}) = \text{trace}(\mathbf{R}_{\boldsymbol{\theta}_k,k|k-1})$, the optimization problem is formulated as

$$\begin{aligned} &\min_{T_s,N_p} \quad \mathcal{G}(T_s, N_p, \hat{w}_{D,k|k-1}) \\ &\text{s.t.} \quad T_s \leq \frac{1}{2\gamma \cdot |\hat{f}_{D,k|k-1}|}. \end{aligned} \tag{15}$$

To solve this, we use `minimize` from `scipy.optimize`, applying sequential least squares programming (SLSQP), a gradient-based method for constrained nonlinear problems. The bounds are set to $[10^{-4},\ 5 \cdot 10^{-3}]$ seconds for T_s and $[64,\ 1024]$ for N_p. At the first timestep, where no prediction exists, we initialize with $T_s = 9 \cdot 10^{-4}$ s and $N_p = 1024$. For subsequent timesteps, the previous solution is used as initialization: $\boldsymbol{\theta}_k = \boldsymbol{\theta}_{k-1}$.

For adaptive ℓ selection in Doppler width estimation, we apply a heuristic rule. Selection among the three different values W_{D1}, W_{D2}, and W_{D3} takes place depending on whether the predicted mean Doppler falls within the ranges $[0, 150]$ Hz, $[150, 300]$ Hz, or above 300 Hz, respectively. This adaptive lag selection improves robustness by decoupling decorrelation from phase wrapping, enhancing Doppler width estimation under varying motion conditions.

V. Simulations and Results

To simulate the evolution of the Doppler parameters, drift coefficients were introduced: $a_f = d_1 \cdot u_f$, $a_w = d_2 \cdot u_w$, where u_f and u_w are drift intensity parameters and $d_1, d_2 \overset{\text{i.i.d.}}{\sim} \{-1, 0, 1\}$ are discrete variables allowing positive, negative, or zero drift. To account for stochastic variability, process noise was also included: the standard deviation of the mean Doppler noise was sampled as $\mathcal{U}(2.0, 6.0)$ Hz and the spectral width noise as $\mathcal{U}(1.0, 3.0)$ Hz. In addition, the number of scatterers M in each scenario was randomly drawn from a uniform distribution: $M \sim \mathcal{U}(8000, 30\,000)$. Considering that we assume $A_m = 1,\ \forall m \in M$, the SNR observed in the experiments varies with the noise level, attaining values as low as 9.5 dB when $\sigma_\eta = 30$. For this noise variance, for instance, the SNR spans the range 9.5 dB–15.3 dB. Each scenario runs for 200 timesteps ($k = 0 \rightarrow 199$), with $\Delta t = 60$ s (this translates to 200 scans of a radar having a scan speed of 1 r/min, revolution per minute).

We performed three Monte Carlo (MC) experiments, each consisting of 1000 independent trials, to evaluate the performance of the proposed Doppler-processing methods under a range of realistic operating conditions. The three experiments differ only in the maximum allowed drift and therefore define three drift regimes: *low*, $u_f \sim \mathcal{U}(0, 5 \times 10^{-3})$ Hz/s; *medium*, $u_f \sim \mathcal{U}(0, 10^{-2})$ Hz/s; and *high*, $u_f \sim \mathcal{U}(0, 5 \times 10^{-2})$ Hz/s. On the contrary, the Doppler width drift is always set to $u_w \sim \mathcal{U}(0, 5 \times 10^{-4})$ Hz/s. For each drift regime, the MC experiment was repeated for four noise conditions corresponding to additive white Gaussian noise with standard deviation $\sigma_\eta \in \{0, 10, 20, 30\}$. For every trial, the initial mean Doppler frequency and Doppler spectral width were drawn independently of uniform distributions over physically plausible ranges, specifically $f_D \sim \mathcal{U}(-550, 550)$ Hz and $w_D \sim \mathcal{U}(5, 25)$ Hz. Note that, as drift accumulates over time, the instantaneous Doppler values may exceed these initial bounds in trials with larger u_f.

These randomized parameters ensure a diverse and statistically representative sampling of Doppler environments across the MC runs. Each scenario instance is uniquely seeded in order to additionally preserve reproducibility among experiments. This reproducibility allows revisiting certain interesting scenarios among the MC runs. The MC runs are applied to the adaptive radar with variable lag estimator [see formulations in (6)], the version of the adaptive radar without adapting the lag value, and a more traditional "sit-and-spin," nonadaptive, approach with $T_s = 9 \cdot 10^{-4}$ and $N_p = 1024$.

To evaluate the estimation performance across the MC simulation, we use the mean absolute error (MAE) of each scenario, i.e., for f_D, $\text{MAE}_{f_D} = (1/K) \sum_{k=0}^{K-1} |\hat{f}_D[k] - f_D[k]|$, over the $K = 200$ timesteps of a single MC trial. However, errors due to folding can be very large, making direct comparisons of MAE difficult. Hence, we present the cumulative distribution function (cdf) of the MAE as calculated for each MC experiment individually for $\sigma_\eta = 10$ in Fig. 2. It is noted that the units have been translated to m/s, considering an S-band radar with a wavelength of $\lambda = 0.1$ m. We can clearly see that adapting both the CPI parameters $\boldsymbol{\theta}$ and the lag value ℓ in the PP estimator introduces important performance improvements over not only the nonadaptive case but over the CPI adapting radar as well. In the case of mean Doppler, both adaptive approaches manage to remain unambiguous, hence avoiding large errors.

The empirical CDFs show that the adaptive approaches outperform the nonadaptive baseline: in the top plot, both curves representing the adaptive approaches are shifted left of the nonadaptive curve, indicating a higher probability of attaining small errors and improved reliability; the bottom plot (representing the performance on $\hat{w}_D$) exhibits the same trend but with reduced separation and a more gradual rise, reflecting greater dispersion for $\hat{w}_D$. Increasing drift severity systematically shifts all CDFs to the right (i.e., worse performance). Adaptive methods retain their relative advantage under stronger drift, providing improvements over the seemingly unaffected nonadaptive case. Overall, adaptation improves

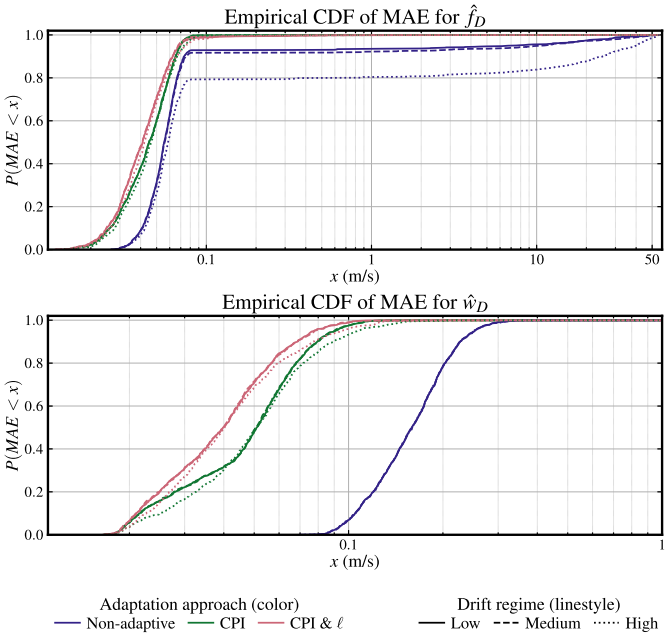

Fig. 2. Empirical CDFs of the MAE for the estimation of f_D (top) and (bottom) w_D. Each colored trace is a measurement approach, and different line styles indicate drift regimes (low, medium, and high). The effect of folding can be seen in the top plot, where errors due to ambiguity produce a nonzero probability of the MAE being as large as 50 m/s for an S-band radar with $\lambda = 0.1$ m.

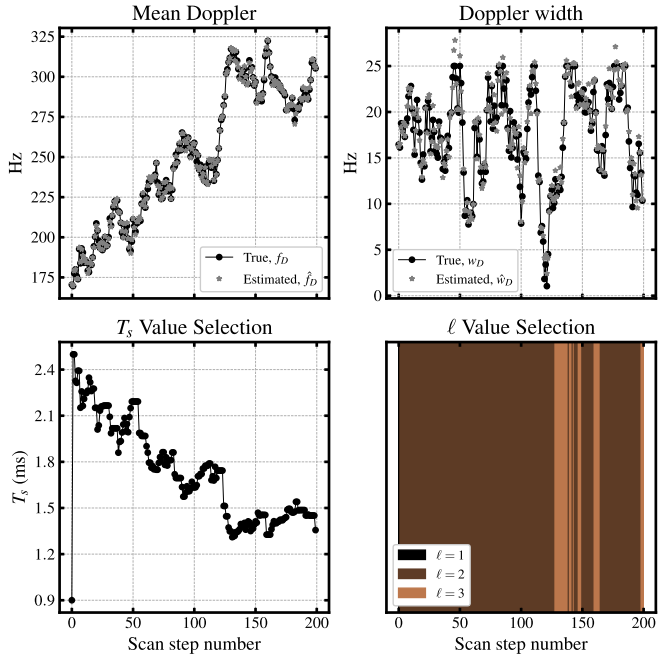

Fig. 3. Handpicked scenario from the MC simulation. (Upper left) Evolution of the mean Doppler drives the adaptation of (lower left) T_s and (lower right) ℓ. (Top right) Additional benefits of the multilag adaptation can be seen in the estimation of w_D. N_p is always assigned the highest possible value. The SNR in this case is equal to 14.73 dB. The experiment starts with $\ell = 1$, switches to 2 for most of the run, and occasionally uses $\ell = 3$ after timestep 125 as the predicted state evolves.

both central tendency and robustness, as folding is avoided even when drift intensifies.

Fig. 3 presents a handpicked case out of the MC runs, where $\sigma_\eta = 30$ and the drift intensity is low. The true value of the mean Doppler f_D can be seen on the top left plot. The way the adaptive radar reacts to those changes can be seen in the lower left and right plots, respectively. Since the number of pulses is not constrained during the optimization, N_p is always assigned the highest value possible and, thus, is omitted from plotting. The radar starts with $T_s = 0.9$ ms, but, from the next scan step onward, it adjusts the pulse repetition time to match the predicted mean Doppler. Similarly, ℓ is also adjusted based on the range of predicted mean Doppler, as explained in Section IV-B, improving the overall performance.

VI. Conclusion

This letter presents initial results for an adaptive radar method to estimate Doppler moments in a single resolution cell of weather radar. We propose an adaptive pipeline, inspired by the FAR framework, which adjusts CPI and estimation parameters (PP correlation lag ℓ). MC simulations show that both adaptive approaches proposed in this work outperform the nonadaptive baseline while remaining unambiguous over time. Hence, severe errors due to aliasing were absent in adaptive methods.

The focus on a single resolution cell of this work serves as proof of concept for the approach. Building on this, future work could involve the expansion of the algorithm to whole scanned sectors or full scans. Moreover, per-target update rate constraints, something that was not addressed in this work, would complicate the problem further, create tradeoffs, and motivate per-sector or per-scan adaptation. Finally, in the case of frequency-modulated continuous-wave radars, where changing the sweep time further affects the maximum range of the radar, an expansion of the optimizer to accommodate additional bandwidth adaptation would be required.

References

[1] M. Steiner, R. A. Houze, and S. E. Yuter, "Climatological characterization of three-dimensional storm structure from operational radar and rain gauge data," *J. Appl. Meteorol.*, vol. 34, no. 9, pp. 1978–2007, Sep. 1995.

[2] R. J. Doviak and D. S. Zrnic, *Doppler Radar & Weather Observations*. New York, NY, USA: Academic, 2014.

[3] D. S. Zrnic, "Estimation of spectral moments for weather echoes," *IEEE Trans. Geosci. Electron.*, vol. GE-17, no. 4, pp. 113–128, Oct. 1979.

[4] K. L. Bell, C. J. Baker, G. E. Smith, J. T. Johnson, and M. Rangaswamy, "Fully adaptive radar for target tracking Part I: Single target tracking," in *Proc. IEEE Radar Conf.*, May 2014, pp. 0303–0308.

[5] T. Dash, H. Driessen, O. A. Krasnov, and A. Yarovoy, "Doppler spectrum parameter estimation for weather radar echoes using a parametric semianalytical model," *IEEE Trans. Geosci. Remote Sens.*, vol. 62, 2024, Art. no. 5100218.

[6] A. E. Mitchell, G. E. Smith, K. L. Bell, A. J. Duly, and M. Rangaswamy, "Cost function design for the fully adaptive radar framework," *IET Radar, Sonar Navigat.*, vol. 12, no. 12, pp. 1380–1389, Dec. 2018.

[7] A. E. Mitchell, G. E. Smith, K. L. Bell, A. J. Duly, and M. Rangaswamy, "Hierarchical fully adaptive radar," *IET Radar, Sonar Navigat.*, vol. 12, no. 12, pp. 1371–1379, Dec. 2018.

[8] P. John-Baptiste, K. L. Bell, J. T. Johnson, and G. E. Smith, "Fully adaptive radar for multiple target tracking," *IEEE Trans. Aerosp. Electron. Syst.*, vol. 58, no. 6, pp. 5749–5765, Dec. 2022.

[9] J. DeLong, M. A. Shattal, A. O'Brien, C. D. Ball, J. T. Johnson, and G. E. Smith, "Fully adaptive cloud profiling radar simulation," in *Proc. IGARSS-IEEE Int. Geosci. Remote Sens. Symp.*, Jul. 2019, pp. 10087–10090.

[10] Y. Bar-Shalom, X. R. Li, and T. Kirubarajan, *Estimation With Applications to Tracking and Navigation: Theory Algorithms and Software*. Hoboken, NJ, USA: Wiley, 2001.

[11] G. Welch et al., "An introduction to the Kalman filter," Tech. Rep., 1995. [Online]. Available: https://www.researchgate.net/publication/200045331_An_Introduction_to_the_Kalman_Filter